

# A Dual-Arm Collaborative Framework for Dexterous Manipulation in Unstructured Environments with Contrastive Planning

Shengzeng Huo, Fangyuan Wang, Luyin Hu, Peng Zhou, Jihong Zhu, Hesheng Wang and David Navarro-Alarcon

**Abstract**—Most object manipulation strategies for robots are based on the assumption that the object is rigid (i.e., with fixed geometry) and the goal’s details have been fully specified (e.g., the exact target pose). However, there are many tasks that involve spatial relations in human environments where these conditions may be hard to satisfy, e.g., bending and placing a cable inside an unknown container. To develop advanced robotic manipulation capabilities in unstructured environments that avoid these assumptions, we propose a novel long-horizon framework that exploits contrastive planning in finding promising collaborative actions. Using simulation data collected by random actions, we learn an embedding model in a contrastive manner that encodes the spatio-temporal information from successful experiences, which facilitates the subgoal planning through clustering in the latent space. Based on the keypoint correspondence-based action parameterization, we design a leader-follower control scheme for the collaboration between dual arms. All models of our policy are automatically trained in simulation and can be directly transferred to real-world environments. To validate the proposed framework, we conduct a detailed experimental study on a complex scenario subject to environmental and reachability constraints in both simulation and real environments.

**Index Terms**—Dexterous Manipulation, Collaborative Action, Unstructured Environments, Planning and Control

## I. INTRODUCTION

**B**IMANUAL manipulation allows to perform more dexterous behaviors than what single-arm systems can do [1]; The availability of an additional arm enables robots to perform various complex long-horizon tasks, i.e., those that require to perform several multi-step subtasks over a long time sequence; Examples of these challenging tasks include assembling furniture [2], spreading a tablecloth [3], grasping and opening a bottle [4], etc. Due to the drastic increase in planning complexity of long-horizon manipulation, the majority of methods further assume rigidity of the manipulated objects and a fully specified goal (e.g. the exact target pose) [5]. However, these assumptions are hard to satisfy in some real-world scenarios. For example, the case where a robot is commanded to pick a deformable cable from a cluttered

environment and arrange it inside a box; The relative spatial relationship “inside the box” represents the desired goal rather than the specific target pose or shape of the cable [6]. Our aim in this paper is precisely to develop methods that break these two assumptions and thus make robot manipulation more applicable for real-world dynamic scenarios, where environmental and reachability constraints are ubiquitous.

Compared with rigid objects, manipulating deformable objects is much more challenging due to their complex mechanical structure (i.e., variable morphology and the high number of degrees of freedom). Although great success has been achieved in managing the high-dimensional configuration of these types of objects with dual arms (e.g. [7]–[9]), shaping deformable objects without a goal specification remains an open research problem. In this paper, we provide a solution to this problem in the context of automatically rearranging a deformable linear object (DLO) in a planar setting while simultaneously satisfying geometric constraints. We choose this case of study since it can be considered a prerequisite for deformable object manipulation (DOM) tasks with fixed contacts [10]–[12]. There are several challenges in this setting: (1) Lack of a goal specification; (2) Nonlinear dynamics of the system in unstructured environments; (3) Long-horizon planning complexity; (4) High-dimensional continuous state-action spaces.

Many researchers have previously addressed the robotic manipulation of soft materials, see [13] for a recent review. However, most existing methods (either model-based [14] or model-free [6], [15]) only consider simple tasks that require few steps. To deal with the complexity of planning long-horizon tasks with DOM, some works have formulated it as a multistep decision-making problem [16]. Point-pair correspondences are utilized in [17] for goal-conditioned control, which requires several intermediate subgoals provided by human demonstration. The planner in [18] exploits an encoder-decoder structure to deal with the high dimensionality of the captured visual observations. However, its generalizability relies on the richness of the collected data. The method in [19] uses the learned object dynamics to implement a simplified version of a Model Predictive Control (MPC) for DOM. However, these types of methods are not able to handle tasks without a complete goal specification.

DOM in unstructured environments is difficult since the actions are constrained and the physical dynamics are complex [10]. There are some works that attempt to solve this challenge

This work is supported by the Research Grants Council (RGC) of Hong Kong under grants 14203917 and 15212721.

S. Huo, F. Wang, L. Hu, P. Zhou and D. Navarro-Alarcon are with The Hong Kong Polytechnic University, Department of Mechanical Engineering, KLN, Hong Kong.

J. Zhu is with the University of York, School of Physics, Engineering and Technology, UK.

H. Wang is with the Shanghai Jiatong University, Department of Automation, Shanghai, China.

without learning the dynamics. However, the majority of them adopt ad-hoc solutions, such as a customized gripper with fixed contacts in [20], task-related action primitives in [21] and simplified state representation with markers in [22]. Other researchers leverage on data-driven methods [23] to avoid modeling the dynamics explicitly. [24] estimates the utility of multiple alternative dynamic models for model-based control. The method in [10] tries to recover from unreliable situations that the unconstrained dynamic model fails. [25] adopts domain randomization techniques to adapt the policy learned in simulation to real situations. However, most of these methods require a great number of resources to learn the complex dynamics in simulation and their performance are affected when they are applied to reality.

To provide a feasible solution to these problems, in this paper we present a novel algorithm for long-horizon bimanual manipulation. In contrast with most algorithms in the literature, our approach does not rely on object rigidity and goal specification assumptions, and can effectively solve diverse tasks under environmental and reachability constraints. As opposed to modeling the complex dynamics of the DLO, our method utilizes spatio-temporal information from previous successful experiences, which enables to transfer the trained policy from simulation to the real world. The cooperative control scheme achieves efficient manipulation with keypoint correspondence-based action parametrization. The original contributions of this work are listed as follows:

- A contrastive learning-based subgoal planner for long-horizon sparse reward tasks without a goal specification.
- A leader-follower control scheme for goal-conditioned collaborative bimanual manipulation under geometric constraints.
- A detailed experimental study that evaluates the proposed method in both simulation and real environments.

The rest of this paper is organized as follows. Sec. II states the problem formulation. Sec. III introduces the state-action parameterization. Sec. IV explains the policy model. Sec. V reports the results and Sec. VI gives the conclusions.

## II. PROBLEM FORMULATION

We formulate the problem as a discrete-time episodic Markov Decision Process (MDP) represented by a tuple  $\mathcal{M} = (\mathcal{S}, \mathcal{A}, R, \mathcal{P}, \rho_0, \gamma, H)$ , where  $\mathcal{S}$  is the state space,  $\mathcal{A}$  is the action space,  $R$  is the reward function,  $\mathcal{P}(S^{[t+1]}|S^{[t]}, A^{[t]})$  is the transition function,  $\rho_0$  is the initial state distribution,  $\gamma$  is the discount factor and  $H$  is the horizon. Instead of shaping a DLO to a specific configuration defined by a compact descriptor (e.g. a contour [15], a pose [5] or an image [21]), the objective of this context is to reach the goal space  $\mathcal{S}_G$ , a subspace of the state space  $\mathcal{S}_G \subseteq \mathcal{S}$  that satisfy geometric conditions. A typical example in Fig. 1 is used to introduce the details, which dual arms are not capable of performing prehensile grasping about the corresponding ends of the DLO in the initial state  $S^{[1]}$  due to the environmental and reachability constraints. Through  $H$  steps of manipulation, the achieved state of the DLO belongs to the goal space  $S^{[H+1]} \in \mathcal{S}_G$ , which means the geometric conditions are

satisfied and the desired grasping is feasible to execute (a real scenario shown in Fig. 1(a)).

As shown in Fig. 1(b), our unstructured environment  $E^{[t]}$  is a rectangle, consisting of a DLO  $L^{[t]}$ , a set of obstacles  $O^{[t]} = \{o_b\}_{b=1}^B$ , and dual robotic arms  $\{a_r\}_{r=1}^2$ . We define the configuration space of an individual robot  $a_r$  as  $\mathbb{C}_r$  and its corresponding valid set as  $\mathbb{C}_r^v \subset \mathbb{C}_r$ . Validity means that the robot is not in collision with the obstacles in the environment  $E^{[t]}$ . Following assumptions about the task are made:

- The binary mask of the DLO  $L^{[t]}$  in the raw visual observation  $I^{[t]}$  can be extracted with a color filter.
- Each obstacle  $o_b$  in the unstructured environment  $E$  is static with the same prior size.
- Both arms  $\{a_r\}_{r=1}^2$  only have partial reachability in the complete planar workspace  $\mathcal{W}$  but share common region, as shown in Fig. 1(c).

$$\begin{aligned} \mathbb{C}_1^v \subset \mathcal{W}, \mathbb{C}_2^v \subset \mathcal{W} \\ \mathbb{C}_1^v \cap \mathbb{C}_2^v \neq \emptyset \end{aligned} \quad (1)$$

- There is always a feasible action  $A^{[t]}$  for the dual-arm system  $\{a_r\}_{r=1}^2$  that deforms the DLO to a new state.

$$\exists A^{[t]} \in \mathcal{A}, S^{[t+1]} = \mathcal{P}(S^{[t]}, A^{[t]}), S^{[t+1]} \neq S^{[t]} \quad (2)$$

- The correspondence between the ends of the DLO  $l_r$  and the individual arms  $a_r$  is known in prior.

The action  $A^{[t]}$  of bimanual manipulation consists of two sequences with respect to dual arms  $A^{[t]} = \{\mathcal{T}_r^{[t]}\}_{r=1}^2$ , where  $\mathcal{T}_r^{[t]} = (P_{pick}, P_{place})$  is a pick-and-place sequence and  $P = [p_x \ p_y] \in \mathbb{R}^2$  is a two-dimension vector representing the 2D position. Note that we ignore the rotation of the gripper and only consider the straight planar displacement during the whole manipulation, in which the z-value depends on the corresponding pixel in the depth map. An action sequence of an arm  $\mathcal{T}_r^{[t]}$  is feasible only if all waypoints inside it  $P \in \mathcal{T}_r^{[t]}$  are within the corresponding valid configuration  $\mathbb{C}_r^v$ , denoted as  $\forall P \in \mathcal{T}_r^{[t]} : P \in \mathbb{C}_r^v$ . Specifically, whether a planar waypoint  $P$  is within the valid configuration  $\mathbb{C}_r^v$  depends on two inequality conditions:

$$P \in \mathbb{C}_r^v \begin{cases} \text{True} & \epsilon_c < |a_r - P| < \epsilon_f \wedge \\ & \epsilon_o < \min_b |o_b - P| \\ \text{False} & \text{else} \end{cases} \quad (3)$$

where  $|\cdot|$  is the  $\mathcal{L}_2$ -distance metric,  $a_r$  and  $o_b$  are the 2D position of  $r$ -th arm and  $b$ -th obstacle and  $\{\epsilon_c, \epsilon_f, \epsilon_o\}$  are corresponding thresholds of the conditions. It is intuitive that if the minimum and the maximum value of the distance between the waypoints  $P \in \mathcal{T}_r^{[t]}$  and the associated instance  $\{P_I|a_r, o_b\}$  in the environment match the aforementioned requirements then the sequence  $\mathcal{T}_r^{[t]}$  is feasible. The maximum value locates on the edge of the straight movement  $D_{max} = \max(|P_I - P_{pick}|, |P_I - P_{place}|)$ , while the minimum value  $D_{min}$  is computed by:

$$D_{min} = \begin{cases} \frac{\overrightarrow{P_1 P_2} \times \overrightarrow{P_1 P_I}}{\|\overrightarrow{P_1 P_2}\|} & \frac{\overrightarrow{P_1 P_2} \cdot \overrightarrow{P_1 P_I}}{\|\overrightarrow{P_1 P_2}\|} < 0 \\ \min(|P_I - P_1|, |P_I - P_2|) & \text{else} \end{cases} \quad (4)$$

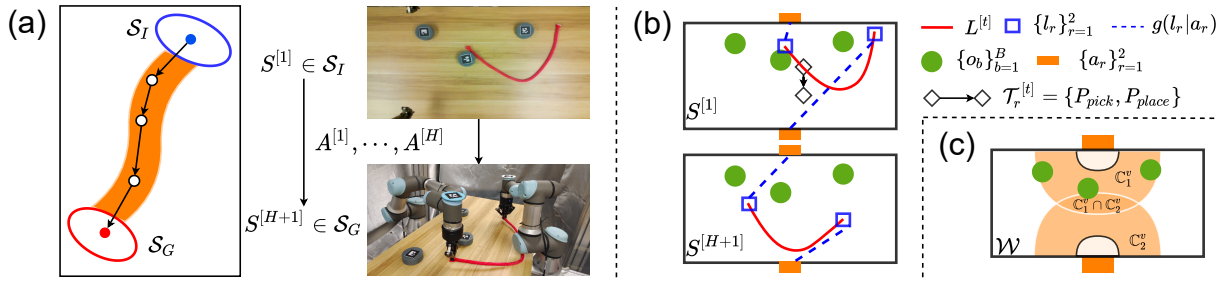


**Fig. 1:** Schematic diagram of our bimanual manipulation setting. (a) Illustration of the context. This task requests robots to rearrange the DLO to enable dual arms to grasp the corresponding ends of the DLO respectively. (b) Graphical representation of the problem formulation. Dual arms are not able to perform prehensile grasping about corresponding ends initially  $S^I$  due to environmental and reachability constraints respectively. Through  $H$  pick-and-place sequences  $\mathcal{T}_r^{[t]}$ , the state of the DLO is transformed as  $S^{[H+1]}$  within the goal space  $\mathcal{S}_G$ . (c) Visualization of the valid configuration space  $\mathcal{C}_r^v \subset \mathcal{C}_r$  of dual arms  $\{a_r\}_{r=1}^2$ . Each arm  $a_r$  only has partial reachability in the complete workspace  $\mathcal{W}$ , while is also limited by the obstacles. Dual arms share common workspace  $\mathcal{C}_1^v \cap \mathcal{C}_2^v$  in the environment.

where  $P_1$  and  $P_2$  represent  $P_{pick}$  and  $P_{place}$  respectively.

The problem we address in this work is how to find a sequence of  $H$  feasible robot actions  $\{A^1, \dots, A^H\}$  under environmental and reachability constraints ( $\forall \mathcal{T}_r^{[t]} : \mathcal{T}_r^{[t]} \in \mathcal{C}_r^v$ ), making the ultimate achieved state of the DLO belongs to the goal space  $S^{[H+1]} \in \mathcal{S}_G$ . As a sparse reward task, the positive signal is returned only when the objective is accomplished, defined as:

$$R(S^{[t]}, A^{[t]}, S^{[t+1]}, \mathcal{S}_G) = \begin{cases} 1, & \text{if } S^{[t+1]} \in \mathcal{S}_G \\ 0, & \text{else} \end{cases} \quad (5)$$

Specifically, the definition of desired states in the goal space  $S^{[t+1]} \in \mathcal{S}_G$  is the endpoints of the DLO located in the valid configuration space of corresponding robotic arms, whose mathematical judgment is:

$$S^{[t+1]} \in \mathcal{S}_G \begin{cases} \text{True} & l_1 \in \mathcal{C}_1^v \wedge l_2 \in \mathcal{C}_2^v \\ \text{False} & \text{else} \end{cases} \quad (6)$$

In summary, the problem we seek to solve is as follows:

$$\begin{aligned} & \text{Find} \quad H, A^1, \dots, A^H \\ & \text{subject to} \quad \forall t \in [1, H] : S^{[t+1]} = \mathcal{P}(S^{[t]}, A^{[t]}) \\ & \quad \quad \quad \forall t \in [1, H] : \mathcal{T}_r^{[t]} \in \mathcal{C}_r^v \\ & \quad \quad \quad S^{[H+1]} \in \mathcal{S}_G \end{aligned} \quad (7)$$

### III. STATE-ACTION REPRESENTATION

#### A. State Parameterization

One critical issue in vision-based manipulation tasks is how to design an efficient descriptor to extract key features from the visual observation  $I^{[t]}$  [26]. We use semantic sequential keypoints [21] for the state representation since they are concise descriptions that allow for an explainable control scheme.

Based on the kinematic multi-body model, we describe a DLO with a link-joint structure and designate the joints as representative keypoints. Similar to our previous work [21], we detect these sequential keypoints  $Q^{[t]} = \{q_k^{[t]}\}_{k=1}^M$  from the mask of the DLO  $L^{[t]}$  in the visual observation  $I^{[t]}$  through a data-driven neural network  $f_D(Q^{[t]}|L^{[t]})$ , which is trained on synthetic data. To simplify the procedures, we render the image-keypoints pair in physical engine Bullet [27], as

opposed to the mathematical Fourier series-based model in [21]. The detailed introduction to the simulation is in Sec. V-A. In addition, another element that influences the policy  $\pi(A^{[t]}|S^{[t]}, \mathcal{S}_G)$  is the obstructions  $O^{[t]}$  in the environment  $E^{[t]}$ . In order to make all the inputs share a common scale without distorting differences in the range of values or losing information, we use the coordinates of the obstacles under observation as their representations. To summarize, we capture the raw image  $I^{[t]}$  at each step  $t$  and extract the mask of the DLO  $L^{[t]}$  with a color filter. Next, we detect the successive keypoints  $Q^{[t]} = f_D(L^{[t]})$ ,  $Q^{[t]} = \{(q_{ku}, q_{kv})\}_{k=1}^M \in \mathbb{R}^{M \times 2}$  and locate the obstacles  $O^{[t]} = \{(o_{bu}, o_{bv})\}_{b=1}^B \in \mathbb{R}^{B \times 2}$ , where  $u$  and  $v$  are 2D coordinates in image. Hence, the representation model  $f_R(S^{[t]}|I^{[t]})$  describes the state  $S^{[t]}$  of the environment  $E^{[t]}$  as  $S^{[t]} = (Q^{[t]}, O^{[t]}) \in \mathbb{R}^{(M+B) \times 2}$ .

#### B. Action Parameterization

The unreasonably vast space of potential actions to complete the goal, encompassing discrete grasping points and continuous motion, is one of the challenges with the policy model  $\pi(A^{[t]}|S^{[t]}, \mathcal{S}_G)$ . In order to reduce the cost of exploration, we formulate the pick-and-place sequence of an arm  $\mathcal{T}_r^{[t]} = \{P_{pick}, P_{place}\}$  as correspondence-based manipulation from the present state  $S^{[t]}$  to the intended state  $S^*$ . The picking and placement locations are specifically chosen inside the keypoints of the present state  $P_{pick} \leftarrow q_k^{[t]} \in Q^{[t]}$  and the intended state  $P_{place} \leftarrow q_k^* \in Q^*$ , respectively. The movement displacement is restricted to not exceed  $\epsilon_D$  in order to prevent a significant change during consecutive moments. As a result, the definition of a pick-and-place sequence for an arm is given as follows:  $\mathcal{T}_r^{[t]} = (q_k^{[t]}, q_k^{[t]} + \min(\epsilon_D, \|\vec{V}\|) \cdot \vec{V})$ , where the moving direction is  $\vec{V} = q_k^* - q_k^{[t]}$ .

### IV. POLICY MODEL

In this section, we explain how to learn the policy model  $\pi(A^{[t]}|S^{[t]}, \mathcal{S}_G)$  to reach the goal space  $\mathcal{S}_G$ , which maps the current state  $S^{[t]}$  to the action  $A^{[t]}$ . Due to the long-horizon planning complexity without a goal specification, sampling efficiency is relatively poor in this sparse incentive environment. To solve this issue, we factorize the policy

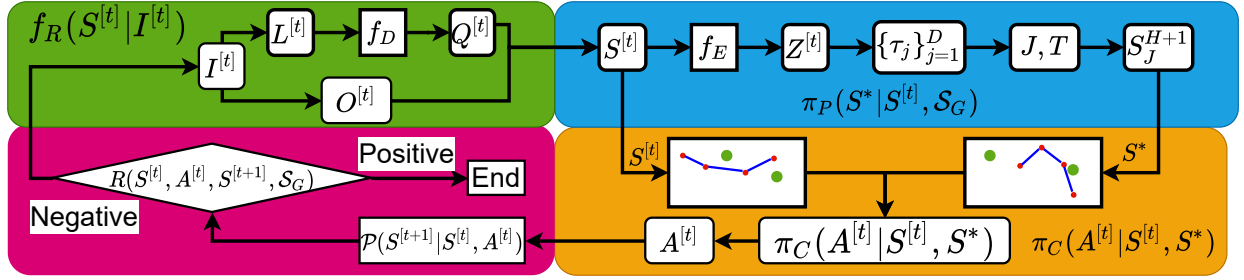


**Fig. 2:** Overview of the proposed planning and control framework. Given the raw observation  $I^{[t]}$  at time step  $t$ , the representation model  $f_R(S^{[t]}|I^{[t]})$  extracts the state  $S^{[t]}$  of the environment  $E^{[t]}$ . The policy model  $\pi(A^{[t]}|S^{[t]}, \mathcal{S}_G)$  consists of two modules, global subgoal planning  $\pi_P(S^*|S^{[t]}, \mathcal{S}_G)$  and local goal-conditioned control  $\pi_C(A^{[t]}|S^{[t]}, S^*)$ . Dual arms execute the action  $A^{[t]}$  and the environment transits to  $\mathcal{P}(S^{[t+1]}|S^{[t]}, A^{[t]})$ . The entire policy iterates until the positive reward  $R(S^{[t]}, A^{[t]}, S^{[t+1]}, \mathcal{S}_G)$  is obtained.

$\pi(A^{[t]}|S^{[t]}, \mathcal{S}_G)$  into global subgoal planning  $\pi_P(S^*|S^{[t]}, \mathcal{S}_G)$  and local goal-conditioned control  $\pi_C(A^{[t]}|S^{[t]}, S^*)$ , which planning here is utilized to offer a promising and practicable detailed goal  $S^*$  for the local controller to pursue, as shown in Fig. 2. Note that we do not need to design an optimal controller to reach each subgoal exactly; instead, the planner points out the promising direction for the control scheme to move. In the following, we first introduce the procedures of data collection in simulation without human participation. Then, we explain how to train the models of subgoal planning based on the collected dataset and the details of the goal-conditioned controller. At last, we explain the pipeline of the policy implementation in real-time after training.

### A. Data Collection

We collect the exploratory experiences of robots via simulation since real-world data on robots is costly. It should be noted that the simulation provides direct access to the state  $S^{[t]}$  of the environment  $E^{[t]}$ . The details about the description of the environment and the manipulation of the DLO are described in Sec. V-A.

As a long-horizon task, an entire state-action trajectory of an episode  $\tau = ([S^{[1]}, A^{[1]}, S^{[2]}, \dots, A^{[H]}, S^{[H+1]})$  involves sampling actions and record the observed states to form trajectories. Since our pick-and-place sequence  $\mathcal{T}_r^{[t]} = (P_{pick}, P_{place})$  is determined based on the current state  $S^{[t]}$  and a desired goal  $S^*$ , we record  $G$  states within the goal space  $\mathcal{S}_G$  to form a dataset  $\{S_g^* \in \mathcal{S}_G\}_{g=1}^G$  through transforming the DLO with arbitrary actions (including picking points and displacements).

In order to avoid time-consuming human supervision, we implement the correspondence-based action randomly based on the goal dataset  $\{S_g^* \in \mathcal{S}_G\}_{g=1}^G$ . The procedures of an episode include choosing a goal  $S_g^*$  within the dataset  $\{S_g^*\}_{g=1}^G$  and sample feasible actions from the correspondence-based parameterization to execute iteratively. Such arbitrary explorations in planning and control unavoidably generate sub-optimal episodes in the dataset  $\mathcal{D}$ , resulting to a sub-optimal policy model  $\pi(A^{[t]}|S^{[t]}, \mathcal{S}_G)$  training on it. To remedy this problem, we explore several times for an episode  $\tau_j$  instead of a single trial. Specifically, we explore  $\epsilon_P$  subgoals in  $\{S_g^* \in \mathcal{S}_G\}_{g=1}^G$  and correspondingly implement  $\epsilon_C$  times goal-conditioned control for each goal. Among the exploration

experiences with  $\epsilon_P \times \epsilon_C$  episodes, we save the one with the minimum horizon. Finally, we obtain a dataset  $\mathcal{D}$  automatically with  $D$  successful episodes  $\mathcal{D} = \{\tau_j\}_{j=1}^D$ , where an episode is  $\tau_j = \{[S_j^{[1]}, A_j^{[1]}, S_j^{[2]}, \dots, A_j^{[H]}, S_j^{[H+1]})\}$ .

### B. Global Subgoal Planning

The aim of the subgoal planner  $\pi_P(S^*|S^{[t]}, \mathcal{S}_G)$  is to point out a promising direction towards the goal space  $\mathcal{S}_G$  for the query state  $S^{[t]}$  rather than to explicitly produce a configuration to attain. However, it is impractical to create a subgoal  $S^*$  from scratch for three reasons. First, the state of the DLO  $S \in \mathcal{S}$  is high-dimensional under certain physical restrictions. Second, the dynamics of a DLO in an unstructured context are highly sophisticated. Third, given non-linear environmental and reachability limitations, it is challenging to determine the achievability between an initial state and a goal state. As a result, we formulate the subgoal planning problem as searching a suitable state from previous exploration  $S \in \mathcal{D}$ . The benefit of this concept is that we can simply transfer the planner from simulation to reality since there is no need to learn the exact dynamics in this complicated environment.

The motivation of our search-based subgoal planner is the ultimate accomplished state  $S_j^{[H+1]} \in \mathcal{S}_G$  of a successful episode  $\tau_j$  is a desirable and feasible goal for the states within this episode  $\{S_j^{[t]}\}_{t=1}^H \in \tau_j$ . Based on this understanding, the obvious strategy for subgoal planning is to find a state in the dataset  $S \in \mathcal{D}$  that corresponds to the present state  $S^{[t]}$ . However, it is challenging to acquire a state in the dataset that is exactly the same as the query in the continuous high-dimensional state space.

Hence, we convert the matching issue during the searching process to clustering within different episodes in the dataset  $\{\{S_j^{[t]}\}_{t=1}^{H+1}\}_{j=1}^D \in \mathcal{D}$ . The states from different episodes are likely to have comparable properties in the original geometric space, making a direct grouping of the states impractical. To deal with these issues, we utilize a data-driven encoder  $f_E(Z^{[t]}|S^{[t]})$  that maps a state  $S^{[t]}$  in the geometric space to an embedding  $Z^{[t]}$  in the latent space.

We train our encoder  $f_E(Z^{[t]}|S^{[t]})$  via a contrastive-learning manner [19], whose key idea is to make the positive pairs of samples disperse closer while the negative pairs diffuse farther. This setting allows us to re-distribute the samples in

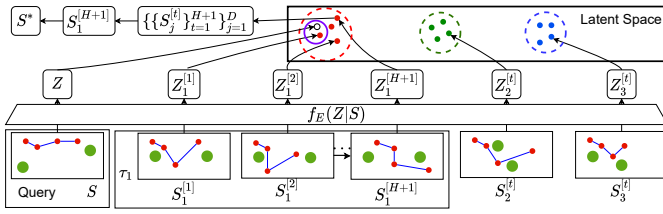


**Fig. 3:** Conceptual representation of our contrastive subgoal planning model. Training data of the embedding model consists of  $D$  trajectories  $\{\{S_j^{[t]}\}_{t=1}^{H+1}\}_{j=1}^D$ . The objective of the contrastive loss is to bring the positive embedding pairs (belong to the same  $j$ -th episode) closer together and the negative embeddings (other states in the dataset  $\mathcal{D}$ ) further away.

the space in accordance with our desired criteria. Also, it is straightforward to employ a universal measure to assess the similarity between samples without task-specific information in the latent space.

The concept of the training and prediction of the contrastive learning-based subgoal planner is illustrated in Fig. 3. For a state in the dataset  $S_j^{[t]} \in \{\{S_j^{[t]}\}_{t=1}^{H+1}\}_{j=1}^D$ , its positive samples are other states belong to the same episode  $\{\{S_j^{[t]}\}_{t=1}^{H+1} \setminus S_j^{[t]}\} \in \tau_j$  while its negative samples are other states in the dataset  $\mathcal{D} \setminus \{S_j^{[t]}\}_{t=1}^{H+1}$ . Notice that the positive and negative associations are not absolute, but rather relative. We choose a positive state  $\bar{S}$  and  $N$  negative states  $\{\tilde{S}_n\}_{n=1}^N$  from the corresponding set for each training with regard to a state  $S_j^{[t]} \in \mathcal{D}$ . With these pairs, we leverage InfoNCE loss [28] to train the encoder  $f_E(Z^{[t]}|S^{[t]})$ :

$$\mathcal{L}_{NCE} = -\mathbb{E}_{\mathcal{D}} \frac{f_H(f_E(S_j^{[t]}), f_E(\bar{S}))}{\sum_{n=1}^N f_H(f_E(S_j^{[t]}), f_E(\tilde{S}_n))} \quad (8)$$

$N$  is the number of negative samples and  $f_H$  is the similarity metric in the embedding space, which we choose bilinear cross product here:

$$f_H(Z_1, Z_2) = \exp(Z_1^T \cdot Z_2) \quad (9)$$

The motivation behind this learning objective lies in maximizing mutual information between the predicted encodings belonging to the same episode. Within the embedding space, this results in the states belonging to the same episode pairs being placed together but the negative samples pushed further apart.

After training the embedding encoding model  $f_E(Z^{[t]}|S^{[t]})$ , the subgoal planner leverages it to plan a subgoal  $S^*$  for the observed state  $S^{[t]}$  during the policy implementation. We first process the states of the collected dataset with the encoding models  $\{\{Z_j^{[t]} = f_E(S_j^{[t]})\}_{t=1}^{H+1}\}_{j=1}^D$ . To clarify the annotations, a state  $S_j^{[t]}$  with  $j$ -th subscript comes from the collected dataset  $\mathcal{D}$  while a state  $S$  is a query during policy implementation. Fig. 3 illustrates how we obtain a subgoal  $S^*$  for a state  $S$  in the query during policy execution. At first, we map it to the latent space through the encoder  $Z = f_E(S)$ . Then, we determine which embedding in the encoded dataset  $\{\{Z_j^{[t]}\}_{t=1}^{H+1}\}_{j=1}^D$  is most similar to it based on the similarity metric  $f_H$ :

$$J, T = \arg \max_{j,t} f_H(Z, Z_j^{[t]}) \quad (10)$$

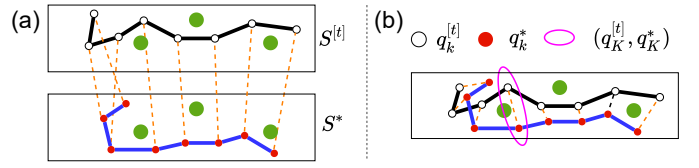


**Fig. 4:** Visualization of the leader-follower control scheme. (a) The keypoints of the current step  $Q^{[t]}$  and the subgoal  $Q^*$  are matched one by one. (b) The search for the leader starts from the keypoints pair with largest  $\mathcal{L}_2$ -norm discrepancy between  $Q^{[t]}$  and  $Q^*$  (shown in purple).

With this equation, we acquire the  $T$ -th state of the  $J$ -th episode in the dataset  $S_J^{[T]} \in \mathcal{D}$  that is most similar to the current state  $S$ . Hence, we assign the ultimate achieved state  $S_J^{[H+1]}$  of the  $J$ -th episode  $\tau_J$  in the dataset as the subgoal for  $S$ , denoted as:  $S^* \leftarrow S_J^{[H+1]} \leftarrow \pi_P(S^*|S^{[t]}, \mathcal{S}_G)$ .

### C. Local Goal-conditioned Control

The local controller  $\pi_C(A^{[t]}|S^{[t]}, S^*)$  is responsible for refining the configuration of the DLO  $S^{[t]}$  based on the subgoal  $S^*$  supplied by the planner model  $\pi_P(S^*|S^{[t]}, \mathcal{S}_G)$ . Note that we do not expressly need the controller to accomplish the subgoal  $S^*$ , but rather to manipulate the DLO to approach it in the promising direction.

Our task is significantly more difficult than conventional single-arm manipulation in structured contexts due to the higher-dimensional discrete-continuous hybrid action spaces for dual arms under reachability and environmental constraints. The following factors must be considered while deciding on the constrained cooperative action  $A^{[t]}$  of dual arms: (1) The choice of a single-arm or bimanual action mode; (2) The assignment of duties between dual arms; (3) The discrete choice of keypoint pairings; (4) The avoidance of collisions when moving two arms simultaneously. To propose an efficient solution addressing these issues, we decouple the roles of twin arms as a leader and a follower [29].

Both the leader and the follower determine the pick-and-place sequence according to the correspondence of keypoints between  $S^{[t]}$  and  $S^*$ , as shown in Fig. 4(a). Without fixed contacts, dual arms adjust their picking points at each time step and their individual roles can be switched. Note that a follower is not guaranteed to participate in this restricted manipulation (thus the system switches to single-arm mode). Both pick-and-place sequences of them are acquired through optimization subject to constraints, which are discussed in detailed in the following.

The objective of the leader is to reduce the error between the current state  $S^{[t]}$  and the subgoal  $S^*$  as much as possible. Hence, we find out the pair of corresponding keypoints with the highest discrepancy in  $\mathcal{L}_2$ -distance:  $K = \arg \max_k \|q_k^* - q_k^{[t]}\|_2$  and the moving direction  $\vec{V}$  of the pick-and-place sequence  $\mathcal{T}^{[t]}$  is:  $\vec{V} = q_k^* - q_k^{[t]}$ , shown in Fig. 4(b). However, the pick-and-place sequence  $\mathcal{T}^{[t]}$  with respect to the specific  $K$ -th pair of keypoints  $(q_K^{[t]}, q_K^*)$  occasionally is not feasible for any arm  $\{a_r\}_{r=1}^2$  in the constrained action space. Therefore, we look for a pair of keypoints  $(q_{K^*}^{[t]}, q_{K^*}^*)$  that is close to the target pair of keypoints  $(q_K^{[t]}, q_K^*)$  while still

allowing an arm to carry out the corresponding pick-and-place sequence. The optimization problem is:

$$\begin{aligned} K^* &= \arg \min_k \|q_k^{[t]} - q_{K^*}^{[t]}\|_2 \\ \text{s.t. } &\exists a_r \in \{a_r\}_{r=1}^2, \forall P \in \mathcal{T}_r^{[t]}, P \in \mathbb{C}_r^v \end{aligned} \quad (11)$$

The chosen arm  $a_r$  in this solution acts as the role of a leader, which implement the pick-and-place sequence  $\mathcal{T}_r^{[t]} = (q_{K^*}^{[t]}, q_{K^*}^{[t]} + \min(\epsilon_D, \|\vec{V}\|) \cdot \vec{V})$ ,  $\vec{V} = q_{K^*}^* - q_{K^*}^{[t]}$  with respect to the  $K^* - th$  keypoint.

Designating one arm as the leader, the other arm naturally acts as the follower. The purpose of the follower is to cooperate with the leader to reshape the DLO as a whole rather than just the surrounding region around the specified  $K^* - th$  keypoint. We search for  $K' - th$  keypoint with the biggest disparity in  $\mathcal{L}_2$ -distance to the chosen  $K^* - th$  keypoint of the leader due to following reasons: (1) deform the DLO globally ; (2) prevent a collision between the leader and follower. In contrast to the leader, the follower's movement direction  $\vec{V}$  is specified in relation to the endpoints around it:  $\vec{V} = l_r^* - l_r^{[t]}$ ,  $r = \arg \min \|l_r - q_k^{[t]}\|_2$ . Taking these into consideration, the optimization problem in terms of the arm acting the role of a follower is:

$$\begin{aligned} K' &= \arg \max_k \|q_k^{[t]} - q_{K^*}^{[t]}\|_2 \\ \text{s.t. } &\forall P \in \mathcal{T}_r^{[t]}, P \in \mathbb{C}_r^v \\ &\|q_{K'}^{[t]} - q_{K^*}^{[t]}\|_2 > \epsilon \end{aligned} \quad (12)$$

where  $\epsilon$  is the minimum distance threshold between the picking points of the leader and the follower to avoid the mutual crash. Note that the role of the follower is eliminated if no available solution is obtained (thus switching to single-arm mode).

In summary, the local goal-conditioned controller  $\pi_C(A^{[t]}|S^{[t]}, S^*)$  outputs the action  $A^{[t]} = \{\mathcal{T}_r^{[t]}\}_{r=1}^2$  to approach the subgoal  $S^*$ , which dual arms  $\{a_r\}_{r=1}^2$  play different roles (leader and follower) for this bimanual manipulation task under environmental and reachability constraints.

#### D. Policy Implementation

---

##### Algorithm 1: Policy Implementation

---

```

while  $R(S^{[t]}, A^{[t]}, S^{[t+1]}, \mathcal{S}_G) \neq 1$  do
   $S^{[t]} \leftarrow f_R(I^{[t]})$ 
   $Z^{[t]} \leftarrow f_E(S^{[t]})$ 
   $J, T \leftarrow \arg \max_{j,t} f_H(Z^{[t]}, Z_j^{[t]})$ 
   $S^* \leftarrow \pi_P(S^*|S^{[t]}, \mathcal{S}_G)$ 
   $A^{[t]} \leftarrow \pi_C(A^{[t]}|S^{[t]}, S^*)$ 
   $S^{[t+1]} \leftarrow \mathcal{P}(A^{[t]}, S^{[t]})$ 

```

---

This section provides an overview of the policy implementation process, which combines global subgoal planning with local goal-conditioned control. The whole policy implementation pipeline is depicted in Alg. 1.

We begin by recording the image observation  $I^{[t]}$  of the unstructured environment  $E^{[t]}$  at each time step  $t$  in

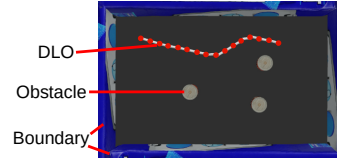


Fig. 5: A snapshot of the simulation.

Paras	Spec.
$\lambda$	$[0.5m, 0.7m]$
$M$	16
$\epsilon_l$	1 rad
$\mu$	0.04
$\epsilon_c, \epsilon_f$	0.15m, 0.45m
$\epsilon_o$	0.1m

TABLE I: Task parameters.

an episode. Next, our representation model  $f_R(S^{[t]}|I^{[t]})$  extracts the state  $S^{[t]}$  through keypoint detection and obstacle localization (Sec. III-A). Second, the subgoal planner  $\pi_P(S^*|S^{[t]}, \mathcal{S}_G)$  obtains a promising and feasible state from the collected dataset  $S_j^{[H+1]} \in \mathcal{D}$  through similarity matching in the latent space, which is encoded by the contrastive learning-based embedding model  $f_E(Z^{[t]}|S^{[t]})$ . Third, taking into consideration the leader and follower roles subject to environmental and reachability constraints, the goal-conditioned controller  $\pi_C(A^{[t]}|S^{[t]}, S^*)$  determines the cooperative action of dual arms  $A^{[t]} = \{\mathcal{T}_r^{[t]}\}_{r=1}^2$ . At last, dual arms  $\{a_r\}_{r=1}^2$  execute the specified action  $A^{[t]}$  to transform the state of the environment from  $S^{[t]}$  to  $S^{[t+1]}$ . The policy replans the subgoal at each step to adapt to the new situation and iterates as a closed-loop control until the acquired state  $S^{[t+1]} = \mathcal{P}(A^{[t]}, S^{[t]})$  corresponds to the goal space  $S^{[t+1]} \in \mathcal{S}_G$  or the maximum limit of the exploration steps  $H_{max}$  is reached.

## V. RESULTS

In order to assess our strategy, we undertake statistical comparisons of our technique against baselines and ablations in the setting of constrained bimanual manipulation. We begin by outlining the simulation conditions and an analysis of our framework that interleaves planning and control using an ablation study. Then we compare our proposed complete framework with several baselines. Finally, we demonstrate the performance of our approach in real-world situations without any fine-tuning.

#### A. Simulation Setting

Data-driven robotics has utilized simulation extensively, but few of them include deformable objects. Through Pybullet [27], [30] represents a DLO as a sequence of rigid bodies subject to the limitations of a fixed distance between adjacent bodies. However, such an articular structure neglects the angular damping and elasticity of DLOs, deviating its dynamics greatly from actual situations. In our setting, we simulate a DLO with a kinematic link-joint model that the rotation range of a joint is limited within  $[-\epsilon_l, \epsilon_l]$ . Specifically, the model comprises  $M - 1$  equivalent-length links connecting with  $M - 2$  revolute joints, plus two additional virtual joints to represent the endpoints. Visualized in Fig. 5, a DLO with a length of  $\lambda$  and multiple cans with a radius of  $\mu$  serving as obstacles are included in the workspace with a size of  $0.6m \times 1m$ . Table I lists the specification of the physical parameters.

A suction gripper carried by a UR5 robotic manipulator is employed in [30] to manipulate through virtual attachment

restrictions. This approach has two shortcomings: (1) The performance of such restrictions is far from the execution of prehensile grasping in actual scenarios. (2) The efficiency of data collecting is decreased by motion planning of robotic arm. With the link-joint structure, we simulate the multi-body dynamics through applying virtual force, whose configuration characterized by the joints  $\mathbf{q} \in \mathcal{R}^M$  is modeled as [31]:

$$M\ddot{\mathbf{q}} + C\dot{\mathbf{q}} + G + \mathbf{J}^T \mathbf{f}_{ext} + \mathbf{K}\mathbf{q} + \mathbf{D}\dot{\mathbf{q}} = \boldsymbol{\omega} \quad (13)$$

where  $\mathbf{q}, \dot{\mathbf{q}}, \ddot{\mathbf{q}}$  represent joint position, velocity and acceleration.  $M$  is the inertial matrix,  $C$  is the centrifugal and Coriolis forces matrix, and  $G$  is gravitational forces.  $\mathbf{J}^T$  is the transpose of the robot Jacobian and  $\mathbf{f}_{ext}$  is the external force.  $\mathbf{K}$  and  $\mathbf{D}$  are the stiffness and damping of the DLO respectively.  $\boldsymbol{\omega}$  is a vector of joint torques. In manipulation with our proposed leader-follower control scheme, the external force is parameterized by its position and magnitude, which is maintained until the intended displacement distance  $\|\vec{V}\|$  is reached. The designed simulation environment provides effective data for our data-driven model, allowing us to transfer from simulation to real environments without any fine-tuning.

### B. Ablation Study

In this experiment, we first exhibit the manipulation procedure of an episode employing our complete framework, which consists of global subgoal planning  $\pi_P(S^*|S^{[t]}, S_G)$  and local goal-conditioned control  $\pi_C(A^{[t]}|S^{[t]}, S^*)$ . Then, in order to emphasize their excellence and necessity, we conduct ablation research versus individual modules.

A complete episode of our constrained bimanual manipulation is shown in Fig. 6. We describe the environment  $E^{[t]}$  as a state  $S^{[t]}$  based on the visual observation  $I^{[t]}$  at each time step  $t$ . Next, we retrieve the embedding  $Z^{[t]}$  of the state  $S^{[t]}$  with the encoder  $f_E(Z^{[t]}|S^{[t]})$  and then locate the most comparable embedding  $S_J^{[T]}$  in the dataset  $\mathcal{D}$  with Eq. 10. Then, we assign the achieved goal  $S_J^{[H+1]}$  of the  $J$ -th episode in the dataset as a subgoal  $S_J^{[H+1]} \rightarrow S^*$ . At last, the local goal-conditioned controller  $\pi_C(A^{[t]}|S^{[t]}, S^*)$  takes the current state  $S^{[t]}$  and the planned subgoal  $S^*$  as input and output the correspondence-based action  $A^{[t]}$ . The entire planning and control framework iterates until the attached state inside the goal space  $S^{[t+1]} \in S_G$ . Following, we put two ablation case studies into practice concerning the planning and the controller, respectively.

First, we claim that our contrastive learning-based planner is capable of extracting the spatio-temporal information of a successful episode, thus providing an appropriate goal for the controller to explore. To back up this assertion, we contrast four alternative subgoal planners, including: (1) **Fixed**: Pick a fixed subgoal randomly for all episodes; (2) **Random Planning**: Sample a subgoal randomly for each episode; (3) **Template**: Choose a subgoal based on  $\mathcal{L}_2$ -distance metric in geometric space; (4) **Auto-Encoder**: Obtain a subgoal based on  $\mathcal{L}_2$ -distance metric in latent space, whose encoder is trained with a self-reconstruction loss. Note that all these contrast algorithms select a subgoal inside the same collected dataset

**TABLE II:** Quantitative comparisons between different methods in the ablation study regarding planning and control

Planning	Control	Success Rate %	Mean actions	Std actions
<b>Fix</b>	<b>LF</b>	51.3	12.8	7.6
<b>RP</b>	<b>LF</b>	50.5	12.8	7.7
<b>Template</b>	<b>LF</b>	72.5	9.7	7.2
<b>Auto-Encoder</b>	<b>LF</b>	69.8	10.2	7.3
<b>Contrastive</b>	<b>OL</b>	78.4	10.1	6.5
<b>Contrastive</b>	<b>RC</b>	79.0	10.1	6.5
<b>Contrastive</b>	<b>LF</b>	<b>86.6</b>	<b>8.0</b>	<b>6.0</b>

**RP:** Random Planning; **LF:** Leader-Follower; **OL:** Only Leader; **RC:** Random Control.

$\mathcal{D}$  and our proposed leader-follower controller is followed to finish the task.

These comparisons are being made to indicate how important a proper subgoal is for the goal-conditioned controller to complete the assignment. The quantitative results of the comparison are shown in Table II and the boxplot comparison is shown in Fig. 7. These results show that our suggested contrastive learning-based approaches get the best success rate among them while demanding the least number of required action steps. To analyze the results, we depict a typical case in the comparisons, as shown in Fig. 8. This example illustrates that the subgoal provided by our contrastive planner is acceptable and points out a promising direction to reach the goal space for the presented state to approach, while other methods are not practical. Without any preference, both **Fix** and **Random Planning** are unable to offer effective and promising subgoals for the controller. **Template** and **AutoEncoder** operate admirably in some circumstances (achieving a success rate of roughly 70% overall), but struggle when the DLO is close to the barriers. The dynamics of the DLO is not smooth as a result of the interactions between it and the fixed obstacles, which makes this mostly plausible. Through clustering the states within an episode together, our contrastive learning-based subgoal planner learns the spatio-temporal representation in the success experiences, namely the feasible and promising transition towards the goal space under constraints. Hence, the intended subgoal is better suited to the query state to approach the goal space  $S_G$ .

Second, we argue that our leader-follower control scheme enhances the goal-reaching capacities of the DLO under environmental and reachability constraints by utilizing the cooperative skills of bimanual manipulation. To substantiate this assertion, we contrast two different controllers, including: (1) **Random Control**: Sample a corresponding-based  $(S^{[t]}, S^*)$  action  $A^{[t]}$  randomly for dual arms  $\{a_r\}_{r=1}^2$ . (2) **Only Leader**: Only the leader action in our leader-follower framework is executed (single-arm policy). Note that all of the alternative controllers execute the action with the same distance threshold  $\epsilon_D$  under constraints and obtain subgoals depending on our proposed contrastive learning-based planner.

The comparisons are made in order to show how effective our leader-follower system is in achieving goal-conditioned control. The quantitative results of the comparison are shown in Table II and the boxplot comparison is shown in Fig. 7. These findings show that among them, our suggested leader-

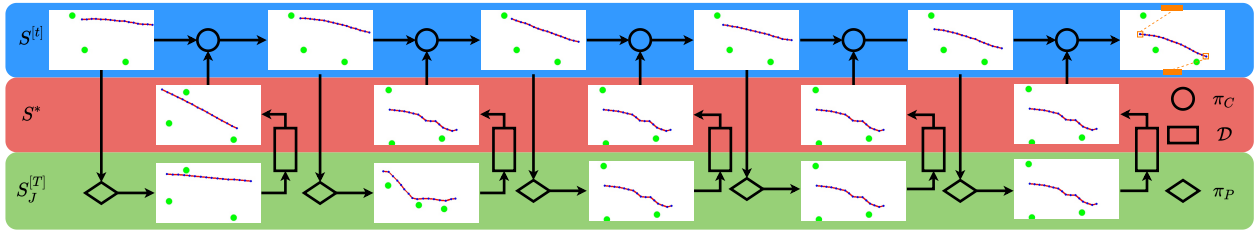


**Fig. 6:** A complete trajectory for an episode within the simulator. At each time step  $t$ , the subgoal planning model  $\pi_P(S^* | S^{[t]}, S_G)$  finds the most similar state  $S_J^{[T]}$  in the dataset  $\{\{S_j^{[t]}\}_{t=1}^{H+1}\}_{j=1}^D$  (green row) concerning the current state  $S^{[t]}$  (blue row) and assign the corresponding achieved goal of the  $J$ -th episode  $S_J^{[H+1]}$  as a subgoal  $S^*$  (red row). Then, the controller  $\pi_C(A^{[t]} | S^{[t]}, S^*)$  determines the action  $A^{[t]}$  conditioning on the current state  $S^{[t]}$  and the subgoal  $S^*$ .

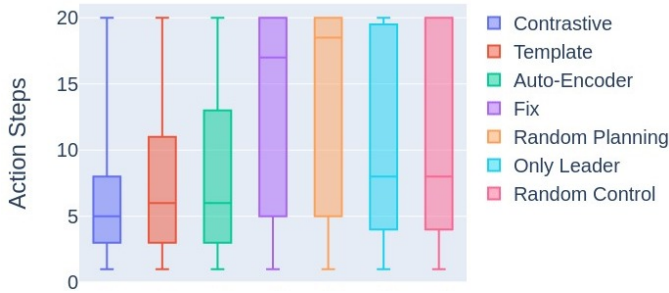


**Fig. 7:** Results of comparisons in the ablation study. The boxplot pictures the required action steps of bimanual manipulation. The central straight line corresponds to the median value of the steps, whereas the sides of the box refer to the first and the third quartiles of the data.

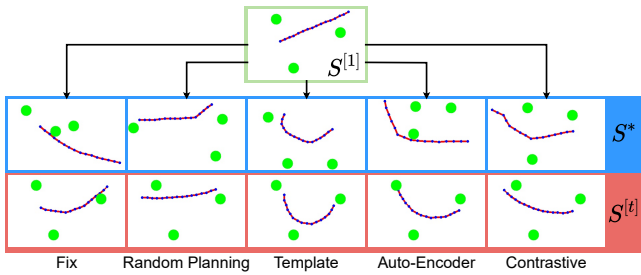


**Fig. 8:** Examples for each of the ablation studies regarding the subgoal selection. All starting from the same initialization state  $S^{[1]}$  (green), different algorithms reach different state  $S^{[t]}$  (red) owing to various subgoals  $S^*$  (blue).

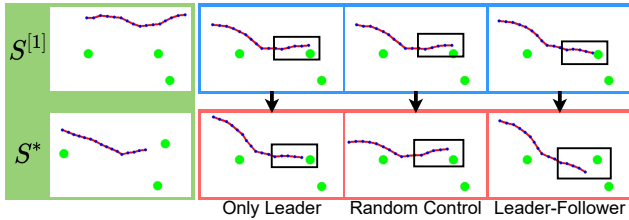


**Fig. 9:** Examples for each of the ablation studies regarding the goal-conditioned controller. All shares the same initialization state  $S^{[1]}$  and the subgoals  $S^*$  (green). Our proposed leader-follower scheme is capable to manipulate the DLO globally to move far from the obstacle (black box), while other baselines perform worse.

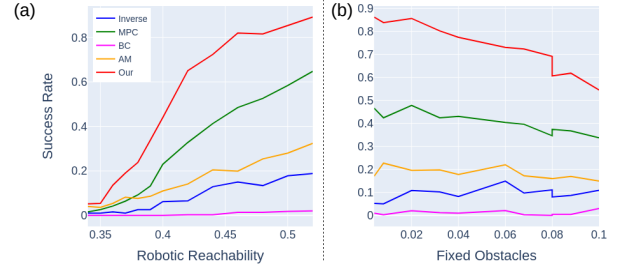


**Fig. 10:** Comparing success rates across methods. (a) The success rate as a function of the reachability of an arm  $\epsilon_f$ . (b) The success rate as a function of the size of individual obstacles  $\epsilon_b$ .

follower scheme has the best success rate while requiring the fewest amount of necessary action steps. A typical example in the comparison is shown in Fig. 9, where each baseline has the identical initial state  $S^{[1]}$  and subgoal  $S^*$ . Moving the right end of the DLO away from the obstruction is the main barrier of the episode (shown in black box). **Random Control** is unable to find the essential components to control because of the arbitrary interests. Even though the fact that **Only Leader** can still alter the key component, it is unable to deform the DLO globally, necessitating extra steps to approach the subgoal. On the contrary, our proposed leader-follower scheme deforms the configuration of the DLO globally with the cooperation between dual arms. This technique effectively alters the DLO toward the subgoal while simultaneously lowering the chance of collision between dual arms.

### C. Comparisons to baselines

The motivations of this work are: (1) Learning the dynamics of managing a deformable object with dual arms in an unstructured environment is challenging, especially when using non-fixed contact; (2) Interleaving planning and control is necessary for a long-horizon sparse reward task without a goal specification. To show the substantial improvements in our methods corresponding to the above arguments, we compare our method against various baselines. For the first claim, we compare our approach to model-based controllers, which rely on knowing the dynamics of the object. Due to the lack of a goal specification, we also train an embedding model  $f_A(S^{[t]}) \approx Z^{[t]}$  to plan a goal  $S^*$  in the latent space, which learns to minimize the  $\mathcal{L}_2$  distance between reconstructed and actual states. Specifically, we find out the achieved embedding



**TABLE III:** Quantitative comparisons between various model-based or model-free baselines

Policy	Success Rate %	Mean actions	Std actions
<b>Inverse</b>	10.5	18.3	5.2
<b>MPC</b>	43.6	14.4	7.3
<b>BC</b>	1.0	19.8	1.5
<b>Action Map</b>	18.0	17.7	5.4
<b>Ours</b>	<b>86.6</b>	<b>8.0</b>	<b>6.0</b>

**Inverse:** Inverse Dynamics; **MPC:** Model Predictive Control; **BC:** Behavioral Cloning.

$Z_j^{[H+1]}$  in the dataset  $\mathcal{D}$  whose  $\mathcal{L}_2$  distance to the encoding  $Z^{[t]}$  of the current state  $S^{[t]}$  is smallest and assign the corresponding state  $S_j^{[H+1]}$  as the goal  $S^*$ . The details of individual model-based controllers are:

- **Inverse Dynamics:** A self-supervised goal-reaching model  $\pi_I(A^{[t]}|S^{[t]}, S^*)$  to perform modeling and control [32].
- **Model Predictive Control:** Based on the forward dynamics model  $f_D(S^{[t+1]}|S^{[t]}, A^{[t]})$ , a sampling-based controller is implemented to achieve one-step optimal predictive control [19].

For the second claim, we compare two model-free techniques that attempt to shorten the distance to the goal space at each step. The details of individual model-free controllers are:

- **Behavioral Cloning** Based on the collected trajectories, the state is mapped to the action  $\pi_{BC}(A^{[t]}|S^{[t]})$  directly in an end-to-end manner [33].
- **Action Map** Similar to FlingBot [34], we predict the values of multiple pre-defined action primitives. Specifically, the action primitives are 8 moving directions with constant displacement discretizing in the planar space and the value function encourages the policy to push the endpoints of the DLO closer to the corresponding arms while shifting away from the obstacles.

All the models are multi-layer perceptrons (MLP) with two hidden layers of size 256 followed by ReLU activation functions. All the baselines share the same state  $S$  provided by our representation model  $f_R(S^{[t]}|I^{[t]})$ , while the action is denoted as two three-dimensional vectors: the first is the index of the pick keypoint on the DLO, and the last 2 are the  $x, y$  delta direction to shape the DLO. In order to compare the baselines fairly, all the dataset used to train the models is explored in the simulation with the same resources, whose action determination is random without human supervision. Owing to the environmental and reachability constraints, the predicted action of the models are adjusted if they are not feasible. Specifically, the search space for the index of the discrete picking points is within  $[-1, 1]$ , while the action is discarded if a feasible one cannot be found within this range. In **Action Map**, all keypoints  $Q^{[t]} = \{q_k^{[t]}\}_{k=1}^M$  are explored for an available solution.

We conduct multiple trials with different robotic reachability ( $\epsilon_f$ ) and fixed obstacle ( $\epsilon_b$ ) settings in order to thoroughly assess the performance of the baselines. Fig. 10 displays the success rates associated with various limitations throughout

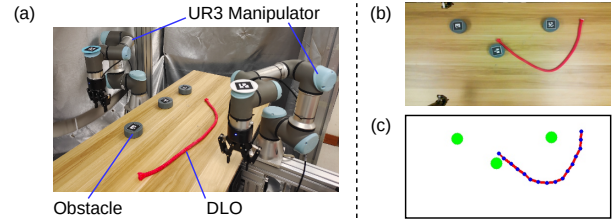


**Fig. 11:** The scenarios of the real environments: (a) Experimental Setup on a planar workspace, consisting of two UR3 manipulators, obstacles and a DLO. (b) Raw visual observation  $I^{[t]}$  provided by the top-down camera. (c) Visualization of the extracted state  $S^{[t]}$  via the representation model  $f_R(S^{[t]}|I^{[t]})$ .

500 experiments. Our proposed algorithm reaches the highest success rate in all settings. Additional quantitative results of a specific setting ( $\epsilon_f = 0.45m, \epsilon_b = 0.04m$ ) are shown in Table III. Our method performs better in terms of three evaluation metrics, success rate, mean action and standard deviation. Without requiring human engineering programming or professional demonstration, our solution always yields satisfactory performance.

In the following, we examine the potential causes of the aforementioned findings. **Inverse Dynamics** do not have a clear aim to infer since there is no particular goal definition. **MPC** outperforms all other baselines because it is effective at reducing the cost of a long-horizon process. However, its performance is affected due to the inaccuracy of the forward dynamics model in this complex configuration. Due to its limited generalization, **Behavioral Cloning** has the weakest performance. In addition, direct end-to-end mapping accumulates errors in the long-horizon procedure. Although **Action Map** compresses the continuous action space by discretization, it simply concentrates on the regional maximum of the value function instead of emphasizing a long-term return. Additionally, this approach necessitates time-consuming human expertise, such as the design of action primitives and task-dependent value functions, both of which are challenging to construct for a sparse reward task in complicated configurations.

#### D. Physical Robot Demonstrations

In this section, we show how well our suggested framework works to transfer from simulation to reality without any fine-tuning. We contend that it is advantageous to interleave planning and control for complicated manipulation tasks with limitations.

Fig. 11 shows our physical robotic environments. Two ur3 manipulators equipped with 2-fingered Robotiq grippers are used for this constrained bimanual manipulation task. The obstacles in the environment are localized with markers and fixed during an episode. An Intel Realsense L515 camera is attached to sense the top-down perspective of the environment  $I^{[t]}$ , as illustrated in Fig. 11(b). Our representation model  $f_R(S^{[t]}|I^{[t]})$  extracts the state  $S^{[t]}$  from the raw observation  $I^{[t]}$ , consisting of sequential keypoints  $\{q_k^{[t]}\}_{k=1}^M$  and fixed obstacles  $\{o_b\}_{b=1}^B$ , visualized in Fig. 11(c).

We implement 100 trials in real-world environments with a success percentage of **90%**. The mean value and standard

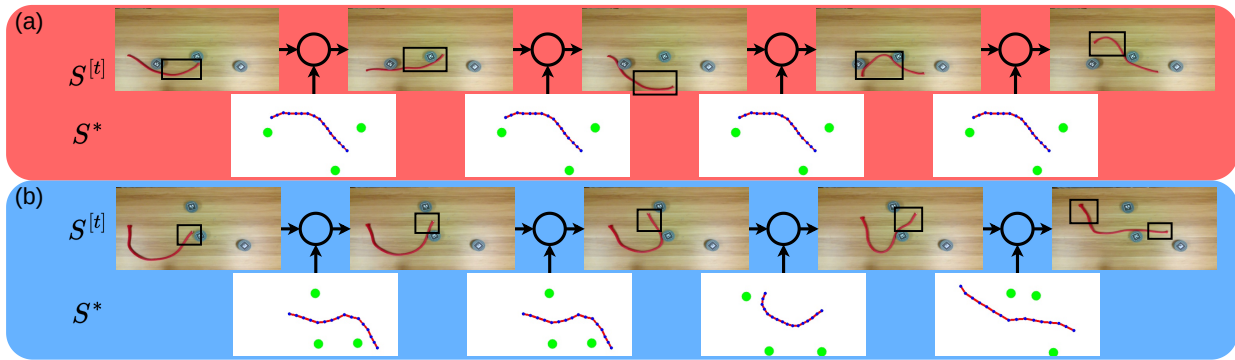


Fig. 12: Pictures of two typical examples in physical robot demonstrations. The black box highlights the manipulated region during action execution.

deviation of actions are **4.48** and **2.79** respectively. Throughout the trials, we make use of the policy model  $\pi(A^{[t]}|S^{[t]}, \mathcal{S}_G)$  trained in simulation and then applied it to actual situations without manual fine-tuning. These findings illustrate that our proposed framework fills out the gap between simulation and real scenarios without any prior knowledge about the physical properties of the deformable object.

To analyze our framework in detail, we provide two typical examples in the trials, visualized in Fig. 12. Fig. 12(a) shows an episode with a constant subgoal that is presented throughout the whole episode. The local goal-conditioned controller initially arranges the DLO to the center of the workspace, allowing dual arms to engage in the subsequent manipulation. The DLO is then adjusted with dual arms, namely rotating it around the obstacle. In order to bypass environmental restrictions, robots finally shift the DLO further from the obstruction. We acknowledge that attached state and the planned subgoal vary in certain ways. Actually, rather than requesting the controller to explicitly attain a particular state, the planner is used to indicate a promising way to approach the goal space. Owing to the replanning operation, the desired subgoal probably varies throughout the episode, as shown in Fig. 12(b). In the beginning, the controller attempts to maneuver the DLO through the barriers by moving it to the right of the workspace. A new subgoal  $S^*$  is included to promote shifting the right end of the DLO to the upper right corner as the state of the DLO changes. Then, both arms participate in distributing the DLO horizontally in the workspace based on a new subgoal  $S^*$ . This example illustrates that replanning is useful to adjust the reaching direction in this challenging constrained bimanual manipulation task.

Although our framework is capable of handling the majority of the challenging tasks, there are some situations when it fails. Fig. 13 presents two typical failure examples. The failure case in Fig. 13(a) is mainly caused by the planner. Our contrastive learning-based planner is driven by a desire to investigate the temporal information about the relative distribution between the DLO and the obstacles in the successful experiences. However, the provided subgoal  $S^*$  is not appropriate for the present state to pursue. Specifically, the obstacles of the episode are in the middle of the workspace, which is a conflict with the subgoal (the obstacles distribute on the side and the major part of the DLO distribute in the middle). The possible

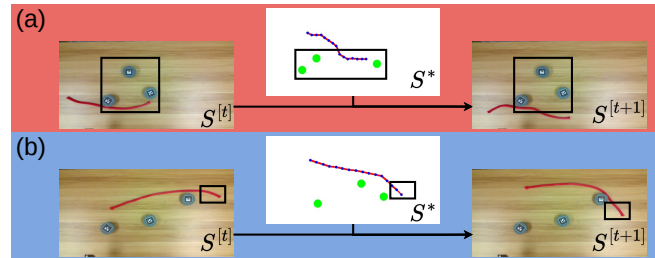


Fig. 13: Pictures of two failed examples in physical robot demonstrations. The black box highlights the focused region when analyzing the cause of the failures.

reason for this phenomenon is our contrastive learning-based encoder  $f_E(Z|S)$  incorrectly classifies certain related states in the latent space. Another failure case in Fig. 13(b) is mainly caused by the controller. The leader-follower control scheme selects the points around the right end to approach the subgoal  $S^*$ . However, this implementation makes the corresponding part of the DLO out of reachability of dual arms, thus failing to manipulate the interested region (around the right end) towards the subgoal  $S^*$  further. As a result, only other areas are accessible for the correspondence-based manipulation, returning the DLO to a state similar to the previous situation. The controller recursively performs the two aforementioned types of actions, namely trapping in this local matching discrepancy.

## VI. CONCLUSION

In this paper, we propose a novel framework for dexterous bimanual manipulation under environmental and reachability constraints. Removing the assumption of object rigidity and a goal specification, our proposed methodology further enhances the intelligence of bimanual manipulation. To deal with the long-horizon complexity, our policy model is factorized into global subgoal planning and local goal-conditioned control. Our subgoal planner provides a promising direction for the state in the query to pursue through similarity matching in the embedding space, which is encoded by an encoder trained in a contrastive learning manner. Our controller leverages a leader-follower scheme to determine the collaborative correspondence-based action of dual arms directed by the subgoal. All the models are trained in simulation and can be transferred to real environments without any fine-tuning.

A detailed experimental study is reported to illustrate the effectiveness of the framework.

However, our methods exhibit some limitations. We choose the state that is closest to the query during each planning, while the uncertainty can not be evaluated. In some situations, the correspondence-based controller traps in a local minimum. For future directions, we are interested to estimate the utility of the subgoal in planning and a feedback-based predictive controller.

## REFERENCES

- [1] S. De Witte, T. Van Hauwermeiren, T. Lefebvre, and G. Crevecoeur, "Learning to cooperate: A hierarchical cooperative dual robot arm approach for underactuated pick-and-placing," *IEEE/ASME Transactions on Mechatronics*, vol. 27, no. 4, pp. 1964–1972, 2022.
- [2] F. Xie, A. Chowdhury, M. C. D. P. Kaluza, L. Zhao, L. L. S. Wong, and R. Yu, "Deep imitation learning for bimanual robotic manipulation," *neural information processing systems*, 2020.
- [3] I. Garcia-Camacho, M. Lippi, M. C. Welle, H. Yin, R. Antonova, A. Varava, J. Borras, C. Torras, A. Marino, G. Alenyà, and D. Kragic, "Benchmarking bimanual cloth manipulation," *IEEE Robotics and Automation Letters*, vol. 5, no. 2, pp. 1111–1118, 2020.
- [4] R. Chitnis, S. Tulsiani, S. Gupta, and A. K. Gupta, "Efficient bimanual manipulation using learned task schemas," *2020 IEEE International Conference on Robotics and Automation (ICRA)*, pp. 1149–1155, 2020.
- [5] A. Simeonov, Y. Du, B. Kim, F. R. Hogan, J. B. Tenenbaum, P. Agrawal, and A. Rodriguez, "A long horizon planning framework for manipulating rigid pointcloud objects," in *CoRL*, 2020.
- [6] D. Navarro-Alarcon and Y.-H. Liu, "Fourier-based shape servoing: A new feedback method to actively deform soft objects into desired 2-d image contours," *IEEE Trans. on Robotics*, vol. 34, no. 1, pp. 272–279, 2018.
- [7] D. Navarro-Alarcon, H. M. Yip, Z. Wang, Y.-H. Liu, F. Zhong, T. Zhang, and P. Li, "Automatic 3-d manipulation of soft objects by robotic arms with an adaptive deformation model," *IEEE Transactions on Robotics*, vol. 32, no. 2, pp. 429–441, 2016.
- [8] M. Yu, H. Zhong, and X. Li, "Shape control of deformable linear objects with offline and online learning of local linear deformation models," in *2022 International Conference on Robotics and Automation (ICRA)*, pp. 1337–1343, IEEE, 2022.
- [9] J. Zhu, D. Navarro-Alarcon, R. Passama, and A. Cherubini, "Vision-based manipulation of deformable and rigid objects using subspace projections of 2d contours," *Robotics and Autonomous Systems*, vol. 142, p. 103798, 2021.
- [10] P. Mitrano, D. McConachie, and D. Berenson, "Learning where to trust unreliable models in an unstructured world for deformable object manipulation," *Science Robotics*, vol. 6, 2021.
- [11] C. Wang, Y. Zhang, X. Zhang, Z. Wu, X. Zhu, S. Jin, T. Tang, and M. Tomizuka, "Offline-online learning of deformation model for cable manipulation with graph neural networks," *IEEE Robotics and Automation Letters*, vol. 7, pp. 5544–5551, 2022.
- [12] J. Zhu, B. Navarro, P. Fraitse, A. Crosnier, and A. Cherubini, "Dual-arm robotic manipulation of flexible cables," in *2018 IEEE/RSJ International Conference on Intelligent Robots and Systems (IROS)*, pp. 479–484, IEEE, 2018.
- [13] J. Zhu, A. Cherubini, C. Dune, D. Navarro-Alarcon, F. Alambeigi, D. Berenson, F. Ficuciello, K. Harada, J. Kober, X. Li, J. Pan, W. Yuan, and M. Gienger, "Challenges and outlook in robotic manipulation of deformable objects," *IEEE Robotics & Automation Magazine*, pp. 2–12, 2022.
- [14] F. Zhang and Y. Demiris, "Learning garment manipulation policies toward robot-assisted dressing," *Science Robotics*, vol. 7, 2022.
- [15] J. Qi, G. Ma, J. Zhu, P. Zhou, Y. Lyu, H. Zhang, and D. Navarro-Alarcon, "Contour moments based manipulation of composite rigid-deformable objects with finite time model estimation and shape/position control," *IEEE/ASME Transactions on Mechatronics*, pp. 1–12, 2021.
- [16] H. Yin, A. Varava, and D. Kragic, "Modeling, learning, perception, and control methods for deformable object manipulation," *Science Robotics*, vol. 6, no. 54, 2021.
- [17] P. Sundaresan, J. Grannen, B. Thananjeyan, A. Balakrishna, M. Laskey, K. Stone, J. E. Gonzalez, and K. Goldberg, "Learning rope manipulation policies using dense object descriptors trained on synthetic depth data," in *2020 IEEE International Conference on Robotics and Automation (ICRA)*, pp. 9411–9418, IEEE, 2020.
- [18] M. Lippi, P. Poklukar, M. C. Welle, A. Varava, H. Yin, A. Marino, and D. Kragic, "Latent space roadmap for visual action planning of deformable and rigid object manipulation," *2020 IEEE/RSJ International Conference on Intelligent Robots and Systems (IROS)*, pp. 5619–5626, 2020.
- [19] W. Yan, A. Vangipuram, P. Abbeel, and L. Pinto, "Learning predictive representations for deformable objects using contrastive estimation," *Conference on Robot Learning*, 2020.
- [20] J. Zhu, B. Navarro, R. Passama, P. Fraitse, A. Crosnier, and A. Cherubini, "Robotic manipulation planning for shaping deformable linear objects with environmental contacts," *IEEE Robotics and Automation Letters*, vol. 5, no. 1, pp. 16–23, 2019.
- [21] S. Huo, A. Duan, C. Li, P. Zhou, W. Ma, H. Wang, and D. Navarro-Alarcon, "Keypoint-based planar bimanual shaping of deformable linear objects under environmental constraints with hierarchical action framework," *IEEE Robotics and Automation Letters*, vol. 7, pp. 5222–5229, 2022.
- [22] D. McConachie, A. Dobson, M. Ruan, and D. Berenson, "Manipulating deformable objects by interleaving prediction, planning, and control," *The International Journal of Robotics Research*, vol. 39, no. 8, pp. 957–982, 2020.
- [23] P. Zhou, J. Zhu, S. Huo, and D. Navarro-Alarcon, "LaSeSOM: A latent and semantic representation framework for soft object manipulation," *IEEE Robotics and Automation Letters*, 2021.
- [24] D. McConachie and D. Berenson, "Estimating model utility for deformable object manipulation using multiarmed bandit methods," *IEEE Transactions on Automation Science and Engineering*, vol. 15, pp. 967–979, 2018.
- [25] J. Matas, S. James, and A. J. Davison, "Sim-to-real reinforcement learning for deformable object manipulation," in *Conference on Robot Learning*, pp. 734–743, PMLR, 2018.
- [26] H. Wang, B. Yang, J. Wang, X. Liang, W. Chen, and Y.-H. Liu, "Adaptive visual servoing of contour features," *IEEE/ASME Transactions on Mechatronics*, vol. 23, no. 2, pp. 811–822, 2018.
- [27] E. Coumans and Y. Bai, "Pybullet, a python module for physics simulation for games, robotics and machine learning," 2016.
- [28] A. van den Oord, Y. Li, and O. Vinyals, "Representation learning with contrastive predictive coding," *ArXiv*, vol. abs/1807.03748, 2018.
- [29] J. Liu, Y. Chen, Z. Dong, S. Wang, S. Calinon, M. Li, and F. Chen, "Robot cooking with stir-fry: Bimanual non-prehensile manipulation of semi-fluid objects," *IEEE Robotics and Automation Letters*, vol. 7, pp. 5159–5166, 2022.
- [30] D. Seita, P. Florence, J. Tompson, E. Coumans, V. Sindhwani, K. Goldberg, and A. Zeng, "Learning to Rearrange Deformable Cables, Fabrics, and Bags with Goal-Conditioned Transporter Networks," in *IEEE International Conference on Robotics and Automation (ICRA)*, 2021.
- [31] P. Chang and T. Padur, "Sim2real2sim: Bridging the gap between simulation and real-world in flexible object manipulation," *2020 Fourth IEEE International Conference on Robotic Computing (IRC)*, pp. 56–62, 2020.
- [32] D. Ghosh, A. Gupta, A. Reddy, J. Fu, C. M. Devin, B. Eysenbach, and S. Levine, "Learning to reach goals via iterated supervised learning," in *International Conference on Learning Representations*, 2020.
- [33] T. Zhang, Z. McCarthy, O. Jow, D. Lee, K. Goldberg, and P. Abbeel, "Deep imitation learning for complex manipulation tasks from virtual reality teleoperation," *2018 IEEE International Conference on Robotics and Automation (ICRA)*, pp. 1–8, 2018.
- [34] H. Ha and S. Song, "Flingbot: The unreasonable effectiveness of dynamic manipulation for cloth unfolding," in *Conference on Robotic Learning (CoRL)*, 2021.